Journal of Hydrology: Regional Studies 51 (2024) 101610

Contents lists available at ScienceDirect

Journal of Hydrology: Regional Studies

journal homepage: www.elsevier.com/locate/ejrh

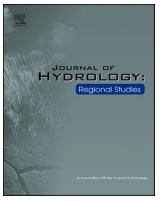

Bias-corrected NASA data for aridity index estimation over tropical climates in Ghana, West Africa

Prince Junior Asilevi [a,b], Felicia Dogbey [b,c], Patrick Boakye [a,d,*], Jeffrey Nii Armah Aryee [b], Edmund Ilimoan Yamba [b], Stephen Yaw Owusu [e], David Kofi Peprah [f], Emmanuel Quansah [b], Nana Ama Browne Klutse [g,h], John Kwesi Bentum [i], Kwaku Amaning Adjei [a], Geophrey Kwame Anornu [a], Sampson Oduro-Kwarteng [a], Leonard Kofitse Amekudzi [b]

[a] *Regional Water and Environmental Sanitation Centre Kumasi, Department of Civil Engineering, Kwame Nkrumah University of Science and Technology, Kumasi, Ghana*
[b] *Department of Meteorology and Climate Science, Kwame Nkrumah University of Science and Technology, Kumasi, Ghana*
[c] *African Regional Centre for Space Science and Technology Education in English, Obafemi Awolowo University Campus Ile-Ife, Nigeria*
[d] *Department of Chemical Engineering, Kwame Nkrumah University of Science and Technology, Kumasi, Ghana*
[e] *Department of Chemistry, Missouri University of Science and Technology, Rolla, MO, USA*
[f] *Department of Information Engineering, Computer Science and Mathematics, University of L'Aquila, Italy*
[g] *Department of Physics, University of Ghana, Legon, Ghana*
[h] *African Institute for Mathematical Sciences (AIMS), AIMS Rwanda Center, KN 3, P.O. Box 71 50, Kigali, Rwanda*
[i] *Department of Chemistry, University of Cape Coast, Cape Coast, Ghana*

ARTICLE INFO

Keywords:
NASA POWER
Water resource
Aridity index
Evapotranspiration
Rainfall

ABSTRACT

Study region: Ghana, West Africa.
Study focus: NASA's Prediction of Worldwide Energy Resource (NASA POWER) satellite-based reanalysis products are used for estimating the aridity index (AI) in Ghana, West Africa. The NASA estimates are compared and bias-corrected with temperature-based potential evapotranspiration estimates and rainfall data from 22 synoptic climate stations. The cumulative distribution function (CDF) matching technique was used for bias correction
New Hydrological Insights for the region: The results indicated a previous 36% over-estimation of arid conditions in dryland climates and an under-estimation of wetland climate regions by the NASA POWER data compared with the station-based estimation. Post bias-correction, the satellite-based estimates showed substantial improvements, as evidenced by a correlation coefficient of $R^2 = 0.87$. The rectified data suggests that with accurate interpretations and calibrations, satellite-based metrics can play a pivotal role in advancing hydrological studies and water resource management in West Africa Sub-region. This insight underscores the potential of satellite data in augmenting regional hydrological research, establishing a foundation for similar studies in analogous global environments.

* Corresponding author at: Regional Water and Environmental Sanitation Centre Kumasi, Department of Civil Engineering, Kwame Nkrumah University of Science and Technology, Kumasi, Ghana.
E-mail address: patrickboakye@knust.edu.gh (P. Boakye).

https://doi.org/10.1016/j.ejrh.2023.101610
Received 13 July 2023; Received in revised form 4 December 2023; Accepted 7 December 2023
Available online 12 December 2023

1. Introduction

Nowadays, freshwater scarcity has emerged as a leading environmental challenge, and efforts to assess and manage water resources is critical for sustainable development (Boltz et al., 2019; Zhang et al., 2020; Mu et al., 2021). Technically, the absolute amount of fresh terrestrial water available to any region for sustainable application is largely an index of the prevailing climate setting (McDonald et al., 2011). Current reports indicate that due to the effects of global warming and climate change, there has been a significant decrease in terrestrial water volume by over 90,000 km^3 . Concurrently, it is observed that nearly 180,000 km^3 of water has become available in different regions over the past 30 years. This redistribution of water resources, which includes increases in some areas at the expense of severe depletions in others, contributes to the complex water crisis affecting many regions, particularly urban areas (Greve et al., 2018; Zhan et al., 2019).

According to Jung et al. (2010) and Oki and Kanae (2006)), nearly 70% of annual cumulative rainfall along with terrestrial water returns to the atmosphere via evaporation and transpiration, which may exceed 95% in arid and arid-prone climates globally. Therefore, evapotranspiration (ET) as an index of the atmosphere's evaporative power and thus the linking mechanism between land surface and the atmosphere is a potential tool for regional water resource monitoring and assessment (Zhan et al., 2019; Mueller et al., 2011; Mueller et al., 2013). As a result, the slightest change in climatic factors such as temperature might create an imbalance in water uptake via ET against precipitation, leading to potential water resource depletion. An accurate knowledge of the spatiotemporal pattern and changes in ET across a region is therefore essential for estimating regional water budgets and developing water management protocols (Anderson et al., 2012; Afzaal et al., 2020). In this regard, an Aridity Index (AI) which incorporates the interplay of rainfall, temperature, and evapotranspiration, was developed as a diagnostic climate index tool, defined based on water availability at a particular location has been used to monitor and predict drought, demarcate desert-sensitive regions, as well as develop water resource management and ecosystem sustainability (McDonald et al., 2011; Nastos et al., 2013; Liu et al., 2013). According to the World Meteorological Organization (WMO) Handbook of Drought Indicators and Indices, a higher Aridity Index value signifies a larger PET compared to precipitation, serving as an indicator of the potential for water scarcity in a region (Moral et al., 2016; Svoboda and Fuchs, 2016).

The Food and Agriculture Organisation's (FAO) Aridity Index (the ratio of mean annual values of rainfall and evapotranspiration) is a widely used method to assess regional spatio-temporal patterns of aridity and water resource availability (Nastos et al., 2013; Bannayan et al., 2010). For example, McDonald et al. (2011) used the FAO AI as a proxy measure to develop a framework for global water availability towards future urban growth, due to limited water data for many regions. Gudmundsson et al. (2016) demonstrated, using probability and statistical analysis, that the sensitivity of water availability to the FAO AI is especially strongest for humid regions. The PET component is usually estimated by the FAO recommended Penman-Monteith equation (FAO 56 PM), computed from four meteorological variables: temperature, relative humidity, wind speed, and solar radiation, found to yield good estimations for a wide range of ecosystems (Córdova et al., 2015; Garcia et al., 2004; López-Urrea et al., 2006; Xing et al., 2008). A major bottleneck, however, is the substantial data requirements which are often unmet due to data scarcity, thus poses application challenge (Stöckle et al., 2004; Trajkovic and Kolakovic, 2009; Li et al., 2012; Rahimikhoob et al., 2012). This is especially the case for developing countries as well as many tropical regions (Droogers and Allen, 2002; Exner-Kittridge and Rains, 2010; Gocic, Trajkovic, 2010; Tabari, 2010; Hou et al., 2013; Wohl et al., 2012). Due to this, a plethora of alternative methods are used. For example, the Hargreaves (Hargreaves et al., 1985) equation allows the estimation of PET based only on temperature data and has been tested for many regions including the Bolivian altiplano (Garcia et al., 2004), Florida (Martinez and Thepadia, 2010), Iran (Fooladmand et al., 2007), Tanzania (Igbadun et al., 2006), and China (Xu et al., 2013). Additionally, satellite-based estimations have emerged as state-of-the-art approaches in recent decades (Moletto-Lobos et al., 2020; Dile et al., 2020).

Given this context, water resource depletion vis-à-vis drought incidence and arable land losses are critical issues for the Southern West Africa (SWA) region, situated between the Gulf of Guinea and the vast Sahara Desert. The region has been identified as particularly vulnerable to global drought, as recent satellite data has indicated a southward extension of the desert by nearly 100 km, exacerbating the ecological stress and contributing to a northward rise in temperatures (Masih et al., 2014; Klutse et al., 2020; Liu, Xue, 2020). The northern half of this region has been identified as most vulnerable to water crisis and drought, primarily due to the increasing heat waves associated with the desert's expansion (Masih et al., 2014). Other studies also show that the southernmost half of the region is equally vulnerable (Rain et al., 2011; Soro et al., 2013).

In light of these pressing challenges, this work endeavored to evaluate the performance of NASA's Prediction of Worldwide Energy Resources (NASA-POWER) gridded satellite-based reanalysis products from for estimating the Aridity Index as a proxy measure of water resource availability within Ghana in the SWA region. The NASA-POWER data developed at the NASA Langley Research Centre provides a wider spatial coverage for temperature and rainfall on a 0.5° geographical coordinate grid globally. First, the products were assessed and bias corrected, to ensure all-round performance evaluation. Secondly, AI was estimated based on PET computed using a Climate Data Toolbox (CDT) script in MATLAB, which is adaptable to different climatic conditions. The performance is based on comparison with AI values estimated from in-situ climate data. At present, this effort is not well explored in the sub-region.

2. Methodology

2.1. Climate and geography of study area

Ghana is a West African coastal country located within latitudes 4.5° N and 11.5° N and longitudes 3.5° W and 1.5° E, and interlocked by Cote d'Ivoire, Togo, Burkina Faso and the Gulf of Guinea to the West, East, North and South respectively. The total land

cover is approximately 240,000 Km^2 and climate is typically tropical monsoon system (Asilevi et al., 2022; Amekudzi et al., 2015). Fig. 1 shows the map of the study area indicating the geographical positions of the twenty-two (22) synoptic stations where temperature and rainfall gauges' measurement datasets were collected.

The broader West African region, characterized by a diverse mosaic of ethnicities and cultures, sustains a population exceeding 380 million (Ahanhanzo et al., 2021). The major livelihood of the populace pivots around agriculture, while the region is fortified by varied reserves of natural resources, vegetation cover, and cash crops such as cocoa. Ghana's ecological tapestry is woven with varied bioclimatic zones: the Coastal Zone featuring mangroves and coastal savannahs, endangered by rising sea levels; the Forest Zone, the green lung housing tropical rainforests, now facing deforestation; the Transition Zone, a blend of woodlands and savannahs; and the Savannah Zone, with its sprawling grasslands, contending with water scarcity (Brandt et al., 2020; Ndehedehe et al., 2019; Du et al., 2019).

The West African Monsoon (WAM) system plays a pivotal role in the region's climate, primarily influenced by the oscillatory migration of the Inter-Tropical Discontinuity (ITD) (Hill et al., 2016; Hill et al., 2018). As a result of this climatic influence, the region distinctly experiences two primary seasons: the wet and the dry. Deepening our understanding, global climate models have underscored the WAM's pronounced sensitivity to atmospheric cloud-radiation interactions (Hill et al., 2016; Danso et al., 2019). Building upon this Asilevi Junior et al. (2022) and Nkrumah et al. (2014) studied the interplay of cloud cover, solar radiation, and precipitation in the region relating to the hydrological system and land-atmosphere-ocean dynamics to understand variations in the Potential Evapotranspiration (PET) across the sub-region.

2.2. Data

2.2.1. Ground-based measurement datasets

For this study, ground measurements were sourced from the Ghana Meteorological Agency (GMet), covering a period of 30 years (1987–2016). The data include daily minimum and maximum air temperatures (T_{min} and $T_{max,}$ °C), relative humidity (RH %), wind speed (u, ms^{-1}), sunshine duration (SD, hours), and rainfall (R, mm). These measurements were collected from 22 distinct synoptic stations, as illustrated in Fig. 1, ensuring a good representation across all four primary climatic zones of the region. GMet oversees the

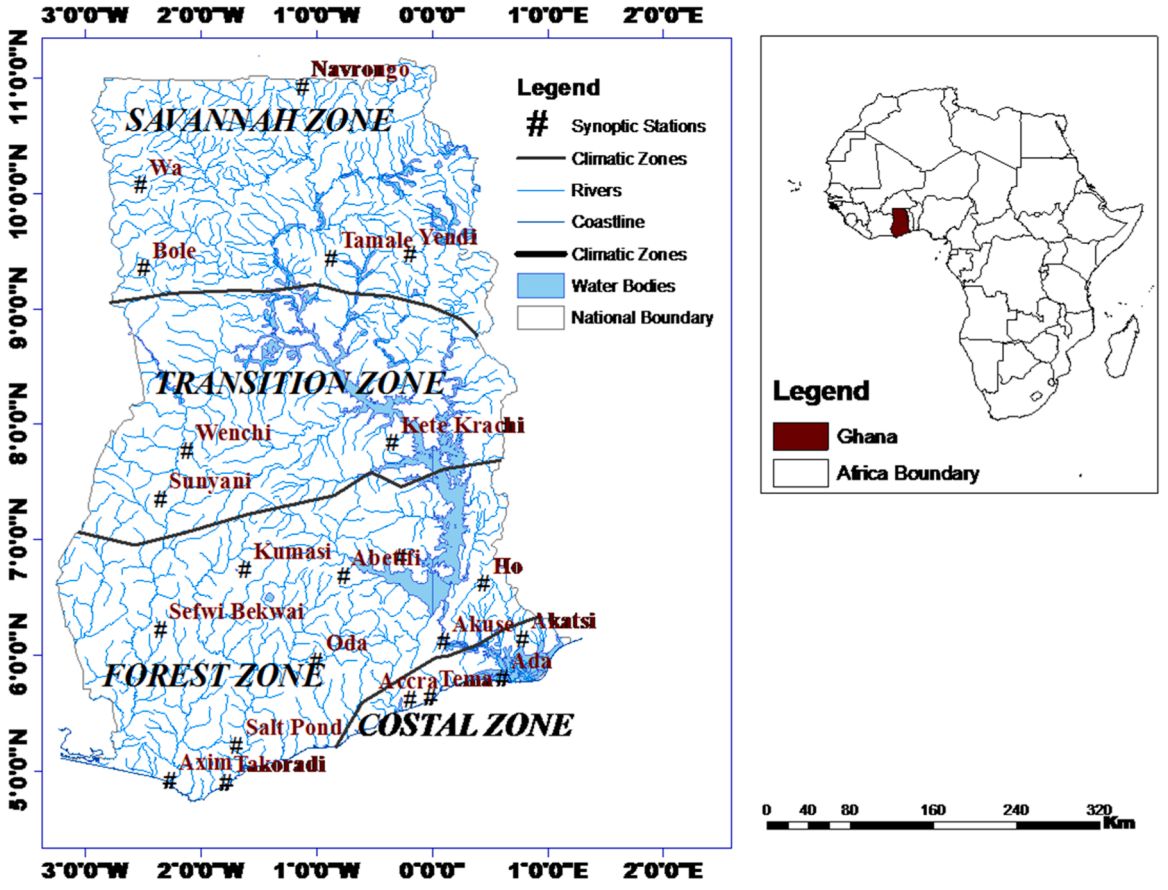

Fig. 1. Hydrological map of study area, Ghana - West Africa, showing network of water bodies across the four main climatological zones, and twenty-two synoptic measurements stations, maintained by the Ghana Meteorological Agency.

collection, quality control, and archiving of measurement datasets. A series of basic quality control checks were further carried out to ensure data accuracy and suitability. First, the relevant period of 1987–2016 was selected based on consistency of data for each parameter, ensuring not > 15% missing data. All outliers were replaced with not available (NA) to compute monthly averages. The daily rainfall datasets were taken with twenty-two (22) gauges mounted at each synoptic station, which have not suffered changes in location. The rainfall datasets were checked to ensure strict adherence to the rainfall climatology: bi-modal and mono-modal rainfall regimes in the southern half (Coastal and Forest zones) and northern half (Transition and Savannah zones) respectively (Asante and Amuakwa-Mensah, 2014).

2.2.2. Satellite-based reanalysis datasets

The satellite-based reanalysis weather products - minimum and maximum air temperatures (T'_{min} and T'_{max}, °C), extraterrestrial solar radiation (H_o, $MJm^{-2}day^{-1}$), and rainfall (R', mm) - spanning equal period as measurement data were retrieved from the National Aeronautics and Space Administration - Prediction of Worldwide Energy Resource (NASA - POWER) agro-climatological repository downloadable via a user friendly web-based mapping portal: https://power.larc.nasa.gov/data-access-viewer/ (Zhang et al., 2008) on a global scale at 0.5° grid area. The NASA-POWER products i.e. T'_{min}, T'_{max}, H_o, and R' are developed from assimilation models based on the Goddard Earth Observing System (GEOS) and the Modern Era Retrospective-Analysis for Research and Applications (MERRA-2) (Rienecker et al., 2011; Suarez et al., 2005). The data assimilation models, based on principles of atmospheric dynamics are used to estimate the weather parameters, relying on atmospheric observations, developed under specific model conditions. The computational models are designed to synthesize and optimize observed and modeled atmospheric variables by incorporating a range of observations including land surface pressure, ocean surface sea level pressure and winds, radar-based sea level winds, upper-air data from radiosondes, drop sondes, pilot balloons, and aircraft winds, atmospheric satellite observations (e.g., moisture profile, total precipitable water, and single level cloud motion vector winds obtained from geostationary satellite images) (Molod et al., 2015; White et al., 2008). Table 1 summarizes the source and temporal coverage for each meteorological parameter.

The reanalysis products have been statistically validated against a global pool of station measurements from the National Center for Environmental Information (NCEI) and the Baseline Surface Radiation Network (BSRN) of the World Radiation Monitoring Center (WRMC), showing reasonable biases less than 15% (Monteiro et al., 2018; Stackhouse Jr et al., 2006). The products have become useful to a broad range of scientists and engineers in renewable energy (Stackhouse Jr et al., 2006) and agriculture (Ojeda et al., 2017; Bai et al., 2010; Savary et al., 2012).

To conduct a comprehensive performance evaluation, the NASA-POWER reanalysis products were first compared with station measurement datasets. The products were then bias corrected to evaluate simulation performance under enhanced conditions. A bias correction technique using Cumulative Distribution Function (CDF) matching was applied to minimize biases for improved representation of local climatology. Basically, the CDF of each station observation data i.e., T_{min}, $T_{max,}$ and R (CDF_o) is plotted along with the corresponding CDF of satellite-based data i.e., T'_{min}, T'_{max}, and R' (CDF'), then the satellite-based data is rescaled according to CDF_o. The difference in their CDFs is plotted against the satellite-based data to fit a polynomial function of nth degree. Then, the inverse CDF of CDF_o gives a final corrected time series of the satellite-based data as shown in Eq. 1 (Singh et al., 2020; Michelangeli et al., 2009).

$$T''_{min}, T''_{max}, R'' = \begin{cases} CDF^{-1}_{T_{min}}\left[CDF_{T'_{min}}\left(T'_{min}\right)\right] \\ CDF^{-1}_{T_{max}}\left[CDF_{T'_{max}}\left(T'_{max}\right)\right] \\ CDF^{-1}_{R'}\left[CDF_{R'}\left(R'\right)\right] \end{cases} \quad (1)$$

where T''_{min}, T''_{max}, and R'' represent the final bias corrected NASA-POWER products, $CDF_{T'_{min}}$, $CDF_{T'_{min}}$, and $CDF_{R'}$ represent the CDFs of NASA-POWER products minimum temperature, maximum temperature, and rainfall respectively.

2.3. Aridity index calculation

The FAO Aridity Index is the ratio of mean annual rainfall (R) and potential evapotranspiration (PET) (McDonald et al., 2011). Table 2 shows the climate-type classification in relation to water availability (McDonald et al., 2011; Moral et al., 2016).

In principle, aridity as a natural phenomenon is a permanent imbalance in the water availability at a location, characterized by low

Table 1
Source and temporal coverage of daily NASA-POWER climatological parameters (White et al. 2008; Monteiro et al. 2018).

Parameter	Source	Temporal coverage	Availability from present data
Daily maximum and minimum temperatures, daily average temperature	Goddard Earth Observing System (GEOS) assimilation model, Version 4 GEOS, Version 5.01 GEOS, Version 5.1	January 1983 to December 2006 January 2007 to December 2007 January 2008 to present	≤ 1 month
Precipitation	Satellite and ground observations from the TRMM and GPCP projects	January 1997 to present	≤ 2 month
Solar radiation	Satellite observations	July 1983 to June 2006; July 2006 to present	≤ 1 month

average annual rainfall, along with high spatio-temporal variability, resulting in overall low moisture and low water carrying capacity of the ecosystem (Pereira et al., 2002). Whereas ecosystems typically exhibit resilience to endemic aridity, substantial deviations from established aridity baselines can destabilize hydrological equilibrium (McDonald et al., 2011; Nastos et al., 2013; Bannayan et al., 2010).

The NASA - POWER datasets i.e., T'_{min},T'_{max}, and H_o were used to compute PET following Hargreaves and Samani (1985) in Eq. 3:

$$PET_{HS} = 0.0135 \times KT/\lambda(T_{mean} + 17.8)(T_{max} - T_{min})^{0.5}H_o \quad (3)$$

where PET_{HS} is the NASA-POWER Hargreaves - Samani based potential evapotranspiration (mm day^{-1}), T_{mean} is the mean of T_{max} and T_{min}, λ is the latent heat of water vaporization (2.45 MJ kg^{-1}), and KT is the adjustable empirical coefficient.

The performance of NASA-POWER products to estimate AI_{FAO} over the study area was evaluated based on AI_{FAO} estimated from the FAO recommended Penman-Monteith equation (FAO 56 PM) shown in Eq. 4 using the station derived datasets i.e., T_{min}, $T_{max,}$ RH, u, SD, and R (Allen et al., 1998).

$$PET_{PM} = \frac{0.408\Delta(R_n - G) + \gamma\frac{900}{T+273}u_2(e_s - e_a)}{\Delta + \gamma(1 + 0.34u_2)} \quad (4)$$

where PET_{PM} is the station based FAO 56 PM evapotranspiration (mm.day^{-1}), R_n is the net radiation at vegetation surface (MJ m^{-2}.day^{-1}), computed according to the method described in Allen et al. G is the soil heat-flux density (MJ m^{-2}.day^{-1}), which according to Allen et al. (1998) can be considered as zero for computation on daily scale, T is the mean air temperature (°C) taken at 2 m height, u_2 is the wind speed taken at 2 m height (ms^{-1}), e_s and e_a are the saturation and actual vapor pressures respectively (kPa), computed from the relative humidity data, (e_s - e_a) is the saturation vapor pressure deficit (kPa), Δ is the slope of the vapor pressure curve (kPa°C^{-1}); and γ is the psychrometric constant (kPa°C^{-1}).

The computations were performed using functional scripts in the Climate Data Toolbox (CDT) for MATLAB, modified and adapted for any climate (Greene et al., 2019).

2.4. Statistical evaluation methods

To evaluate performance of the NASA-POWER reanalysis products against measurement data, the following statistical methods for deviation and correlation analysis in Eqs. 5–7, each showing a complimentary result were used: Standard deviation (σ), Mean bias difference (MBD), and the coefficient of determination (R^2) for n observations.

$$\sigma = \sqrt{\frac{1}{n-1}\sum_{i=1}^{n}(x - \mu)^2} \quad (5)$$

$$MBD = \frac{1}{n}\sum_{i=1}^{n}(x_m - x_{NP}) \quad (6)$$

$$R^2 = 1 - \frac{SS_{res}}{SS_{tot}} \quad (7)$$

where x is the study parameter, x_m and x_{NP} are the station measurement and NASA-POWER derived variables respectively. $SS_{res} = \sum_{i=1}^{n}(x_m - x_{NP})^2$, is the sum of the squares of the differences between the station data and the NASA-POWER data, and $SS_{tot} = \sum_{i=1}^{n}(x_m - \overline{x}_m)^2$, is the sum of the squares of the differences between the observed values and their mean. Here, $\overline{x}_m$ represents the mean of the station data. The arithmetic mean of any dataset is μ (Khosravi et al., 2019).

The standard deviation (σ) was used to check the upper and lower limits of distribution around the mean deviations between the ground data and NASA-POWER reanalysis data in order to ascertain violations between both observations (Mahmoud et al., 2010). The MBD is a good indicator for under or over-estimation in observations, with MBD values closest to zero being desirable. The coefficient of determination (R^2) was used to quantify the degree to which the variance in the ground data can be predicted from the reanalysis dataset (Nagelkerke, 1991; Khosravi et al., 2019).

Table 2
Climate classification according to AI_{FAO} (Moral et al., 2016).

Climate zones Aridity index	
Hyper arid	$AI_{FAO} < 0.05$
Arid	$0.05 \leq AI_{FAO} < 0.20$
Semi-arid	$0.20 \leq AI_{FAO} < 0.50$
Dry sub-humid	$0.50 \leq AI_{FAO} < 0.65$
Wet sub-humid	$0.65 \leq AI_{FAO} \leq 0.75$
Humid	$AI_{FAO} > 0.75$

2.5. Gridding by Inverse Distance Weighting (IDW)

Finally, to develop a spatial appreciation of the estimated Aridity Index across the study area, a spatial interpolation of the data was performed using the Inverse Distance Weighting (IDW) method. Widely used in geographic information systems, this technique generates continuous surfaces from discrete data points and is particularly effective for environmental and atmospheric data (Susanto et al., 2016). IDW operates on the principle that closer points exert greater influence on the interpolated value than distant ones, ensuring an accurate spatial representation of climatic variables (Setianto and Triandini, 2013).

Computationally, the original IDW interpolation technique follows Eqs. 8–10 as presented by Shepard (1968):

$$\hat{z}(x_0) = \sum_{i=1}^{N} \lambda(d_{s_i})_i \bullet v_i \tag{8}$$

$$\lambda(d_{s_i})_i = \frac{d_{s_i}^{-u_s}}{\sum_i^N d_{s_i}^{-u_s}} \tag{9}$$

$$d_{s_i} = \sqrt{(x_i - x)^2 + (y_i - y)^2} \tag{10}$$

A key advantage of the IDW method is its effectiveness in reflecting local variations and trends, making it particularly suitable for

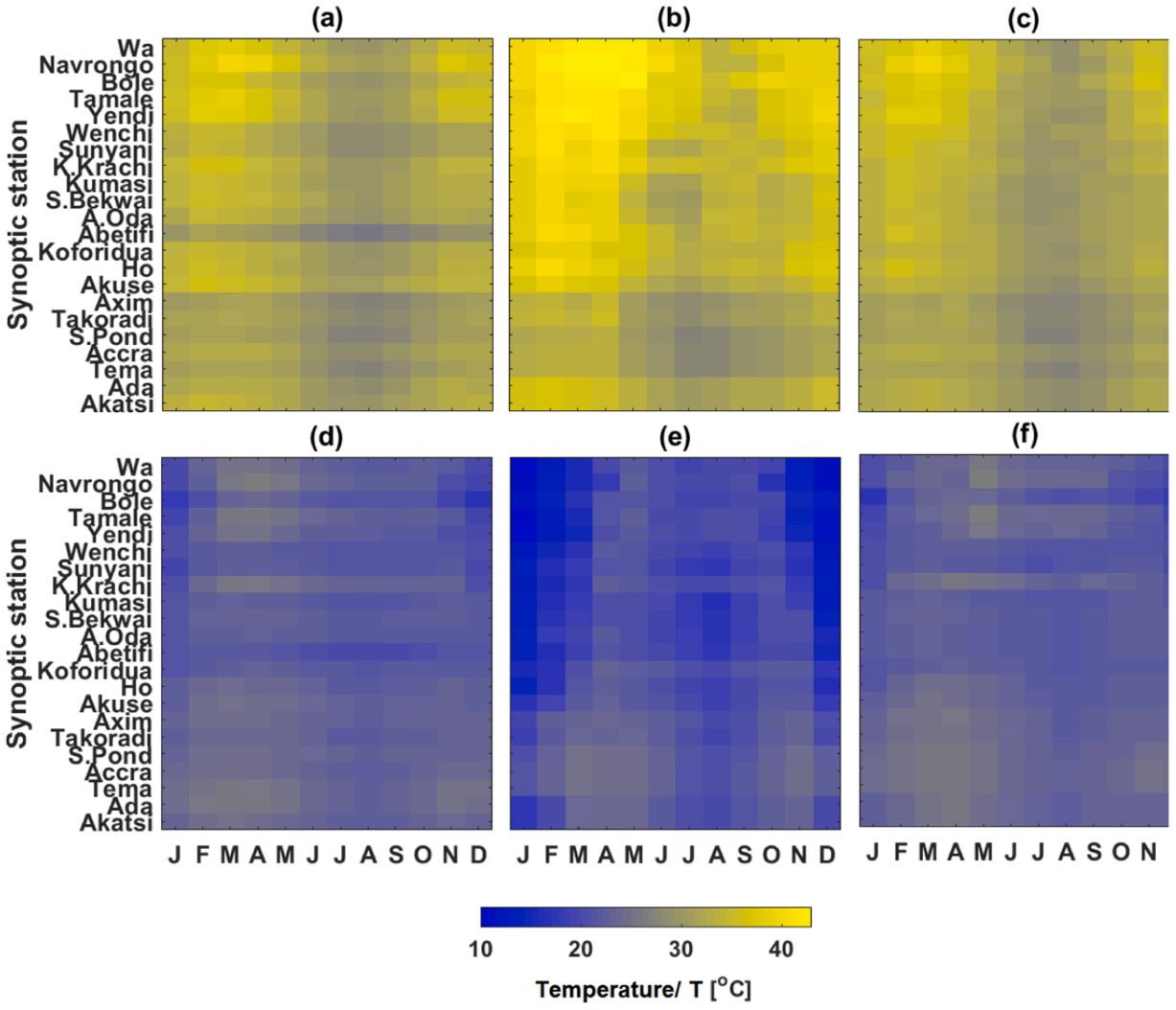

Fig. 2. Spatial distribution of long-term monthly mean (a) station maximum temperature (T_{max}), (b) NASA-POWER maximum temperature (T'_{max}), (c) bias corrected NASA-POWER maximum temperature (T''_{max}), (d) station minimum temperature (T_{min}), (e) NASA-POWER minimum temperature (T'_{min}), and (f) bias corrected NASA-POWER minimum temperature (T''_{min}).

climatological studies.

3. Results and discussions

3.1. Evaluation of NASA-POWER gridded data

Initial analysis centered on the gridded products from NASA's Prediction of Worldwide Energy Resources (POWER) project, utilizing the data to examine regional temperature and rainfall patterns across the study area. The evaluation presented in Figs. 2a - 2f involved a comparison between monthly mean NASA-POWER derived maximum and minimum temperatures (T'_{max},T'_{min}) and ground-based station measurements (T_{max}, T_{min}), with subsequent bias adjustment to the NASA-POWER temperatures (T''_{max}, T''_{min}). The spatial distribution of long-term monthly mean maximum and minimum temperatures revealed distinct seasonal trends, with peaks in T_{max} during February and May, and a significant rise in October-December, which was especially pronounced in the northern half of Ghana. The NASA-POWER data demonstrated a tendency to overestimate T_{max}, with differences ranging from 0.24° to 7.65°C above the station records, particularly notable during the peak seasons. The mean maximum temperature derived from NASA-POWER was consistently higher than the ground-based measurements, with margins of 4.81, 5.46, 3.24, and 0.98 °C for the Savannah, Transition, Forest, and Coastal zones, respectively (Fig. 2b).

After applying bias correction, a notable reduction in the over-estimation was observed, with mean zonal differences of − 0.03, 1.1, 0.1, and − 0.2 °C, respectively (Fig. 2c), indicating an improved alignment with ground-based observations. The adjusted R^2 values also showed a modest enhancement from 0.6 to 0.79, suggesting that the bias correction could help enhance the precision of NASA-POWER temperature data for regional climate studies.

Conversely, the mean minimum temperature from NASA-POWER (T'_{min}) was underestimated, particularly in the Savannah, Transition, Forest, and Coastal zones, by − 5.2, − 4.0, − 2.9, and − 1.5 °C, respectively (Fig. 2e). The bias-adjusted values for T''_{min} (Fig. 2f) displayed a more accurate match with station data, with R^2 improvements from 0.39 to 0.77, underscoring the potential of bias adjustment in mitigating systemic errors in the NASA-POWER dataset.

Comparative analysis with other studies corroborates our findings (White et al., 2008). For instance, the most significant discrepancy in T_{max} (over-estimation of 7.64 °C) was recorded at Abetifi, correlating with its high elevation, while the smallest under-estimation of T_{min} was observed in the mountainous northern half.

This was been attributed to the fact that, NASA-POWER data are representative of mean values for an entire grid area, such that for mountainous areas, the actual station elevation may differ significantly from the mean NASA-POWER grid area elevation (White et al., 2008; Stackhouse Jr et al., 2006). This regional variability accentuates the necessity of localized calibration for global climate models, ensuring their utility and relevance in regional climatological research.

Fig. 3 presents a comparative assessment of long-term monthly mean rainfall across different locations within the study area, as measured by ground stations (Fig. 3a), estimated by the NASA-POWER reanalysis dataset (Fig. 3b), and following bias correction (Fig. 3c). Examination of the spatial and temporal patterns indicates that NASA-POWER rainfall estimates generally exhibit a high degree of congruence with gauge measurements, particularly capturing the overall trend of increasing rainfall from January to the peak in the rainy seasons.

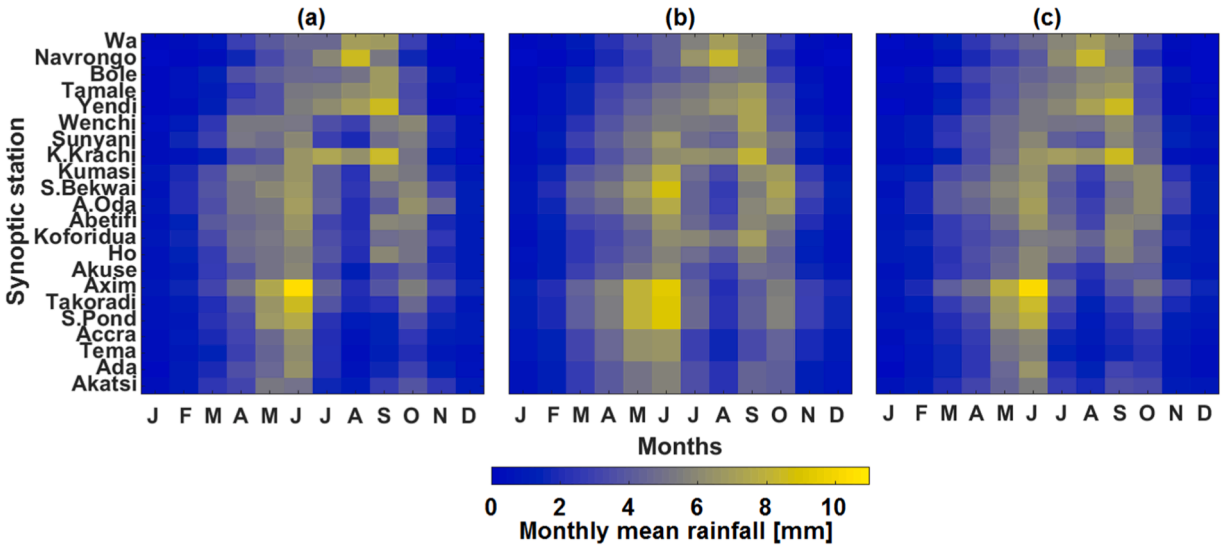

Fig. 3. Spatial pattern of long-term monthly mean rainfall for (a) station gauge measurement, (b) NASA-POWER, and (c) bias-corrected NASA-POWER.

However, certain discrepancies are noticeable between the observed and NASA-POWER data, with NASA-POWER typically overestimating rainfall during the peak rainy months. This is particularly evident over regions that experience a bimodal rainfall pattern, which the raw NASA-POWER data occasionally smears into a less distinct pattern. Following bias correction, there is a pronounced refinement in the representation of these seasonal peaks, enhancing the dataset's fidelity to observed climatology (Asilevi et al., 2022; Hill et al., 2018).

Quantitatively, the original NASA-POWER data showed minor discrepancies, which were addressed through bias correction. This significantly improved the coefficient of determination for rainfall estimates, especially in the northern half of the study area. Such enhancements validate the dataset's applicability for hydrological research once corrected.

Fig. 4 shows the results of bias correction experiments leading to improvement of the NASA-POWER data as displayed in Figs. 2c, 2f, and 3c. Basically, we reduced biases in the reanalysis datasets by cumulative distribution frequency (CDF) matching method with reference to the station datasets. It is seen that reanalysis temperature datasets are the most biased compared to rainfall. For NASA-POWER maximum temperature (T'_{max}), an absolute mean bias of 3.4 °C is reduced to 0.14 °C (Fig. 4a), whereas for NASA-POWER minimum temperature (T'_{min}), an absolute mean bias of 3.2 °C is reduced to 0.12 °C (Fig. 4b), both depicting marginal under-estimation.

In the case of rainfall (Fig. 4c), an initial absolute mean bias of 0.37 mm is reduced to 0.001 mm, commensurate with improved R^2 from 0.85 to 0.93. Table 3 summarizes a comparison of the mean values for both station datasets derived from the GMet and the NASA-POWER reanalysis archives.

Using the bias-corrected data, Climatological Adjustment Factors (CAF) were developed to adapt the gridded NASA-POWER data to local climatology. The mean CAFs for maximum temperatures were 1.14 for Savannah, 1.17 for Transition, 1.11 for Forest, and 1.03 for Coastal zones, while for minimum temperatures, they were 0.76, 0.82, 0.87, and 0.94 for the respective zones. This adjustment

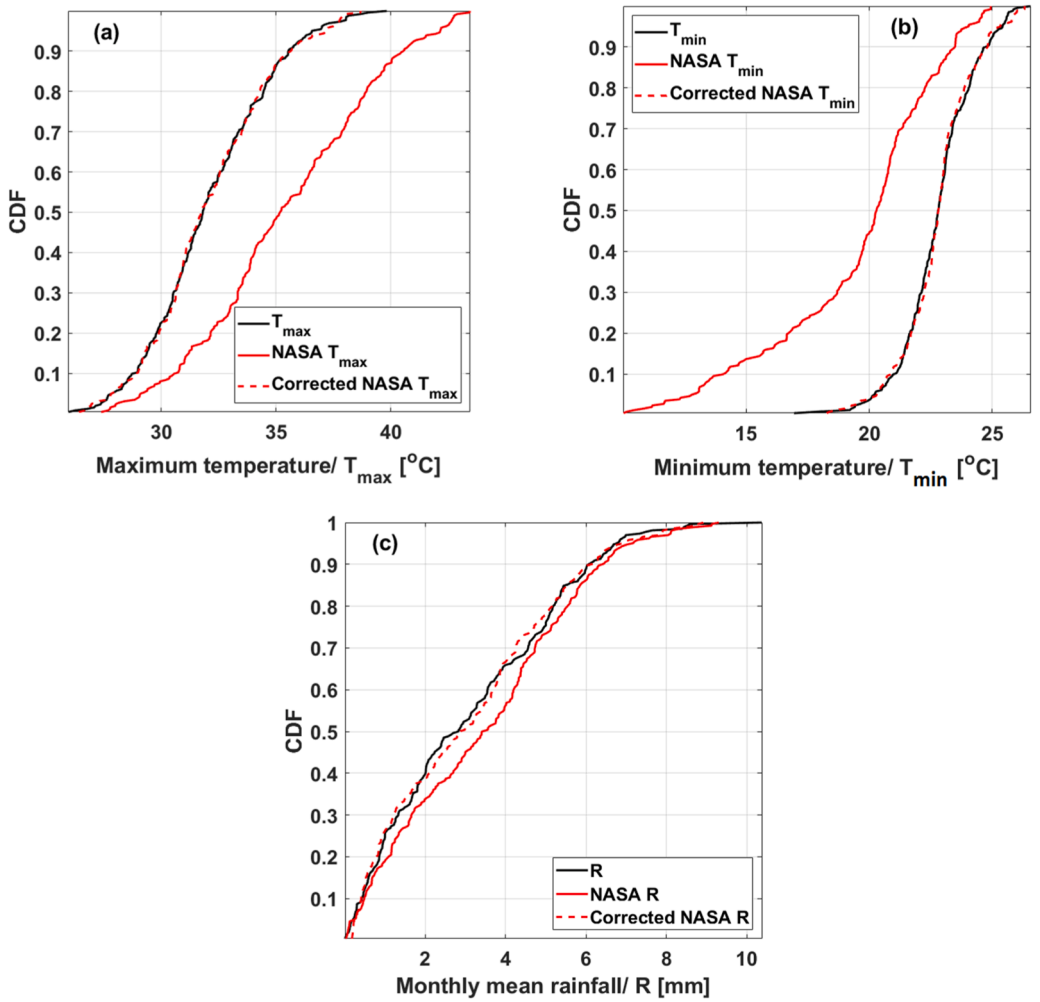

Fig. 4. Improved NASA-POWER reanalysis data by CDF matching technique for (a) maximum temperature (T_{max}), (b) minimum temperature (T_{min}), and (c) rainfall. Black line is the CDF of station measurement data, red line and red dash line are the CDF of NASA-POWER (biased) and bias corrected NASA-POWER datasets.

technique has been used to develop the Climate Data Tool (CDT) by The ENACTS (Enhancing National Climate Services) initiative under the International Research Institute for Climate and Society (IRI) (Dinku et al., 2022) for merging station data and proxy data.

3.2. Performance of NASA-POWER products for AI based water resource assessment

From the initial assessment presented in Section 3.1, the objective of this work is to evaluate the performance of NASA-POWER reanalysis products for Aridity Index -based water resource availability distribution. Fig. 5 compares Aridity Index distribution maps developed from long-term mean evapotranspiration and precipitation datasets derived from station measurements and NASA-POWER based on equation 2. The maps are generated by inverse distance weighting (IDW) in ArcGIS spatial mapping tool version 10.8.

Fig. 5a, which represents the assessment standard, is the FAO Aridity Index (AI_{FAO}) constructed based on the FAO 56 PM evapotranspiration estimated using station data. As shown in Fig. 5a and referencing Table 2, AI_{FAO} ranges 0.47–1.14 representing 77% humid to wet sub-humid climate land area (green) prevalently over the forest climate zone and 23% dry sub-humid to semi-arid land area mainly over the northern Savannah (brown) and pockets of the coastal stretch (red). The as-retrieved NASA-POWER based Aridity Index (AI'_{FAO}) ranging 0.26–0.97 estimated 41% humid to wet sub-humid climate land area covering the south region and 59% dry sub-humid to semi-arid climate land area across the middle and entire northern half (Fig. 5b). The bias corrected NASA-POWER based Aridity Index (AI''_{FAO}) ranging 0.55–1.03 estimated 73% humid to wet sub-humid climate land area and 27% dry sub-humid to semi-arid climate land area (Fig. 5c). In relative terms, AI'_{FAO} overestimated the stretch of dry lands whiles underestimating the stretch of wetlands. Contrarily, the improved AI''_{FAO} showed good agreement with AI_{FAO} with the percentage stretch of wet and dry climate land areas. The improvement in AI''_{FAO} compared with AI'_{FAO} is shown in Fig. 6. As aforementioned, the aridity index distribution is an indicator of water availability or deficit based on the long-term climatological balance between precipitation and evapotranspiration (Moral et al., 2016; Gebremedhin et al., 2018; Tabari et al., 2014).

The AI distribution in Figs. 5a and 5b are more consistent with annual rainfall distribution over the area (Amekudzi et al., 2015; Nkrumah et al., 2014). Climatologically, the southeastern region of Ghana is the rainfall hub of the country, with annual cumulative rainfall reaching 1500 mm (Asante and Amuakwa-Mensah, 2014). Furthermore, the region has the highest mean cloud cover distribution, and consequentially the lowest intensity of solar radiation (Asilevi et al., 2022; Danso et al., 2019). Therefore, these conditions favor a more humid climate hence a high-water availability accurately estimated by AI_{FAO} and AI''_{FAO}. In contrast, the northern half, toward the Savannah region, receives the most solar radiation due to lower cloud cover and higher atmospheric clearness. Moreover, temperatures are relatively higher (Klutse et al., 2020; Asilevi et al., 2022). These conditions accurately explain the levels of aridity and resulting water availability depicted in Figs. 5a and 5b.

The implications based on Fig. 5a are that the semi-arid pocket regions of the Savannah and Coastal climate zones require effective irrigation systems for sustainable agriculture (Gebremedhin et al., 2018). Additionally, NASA-POWER reanalysis products need improvement and site-specific adaptation to better delineate and manage regional water resources. A significant advantage is NASA-POWER's ready availability and the ease of assessing water resources for developing and monitoring aridity on a regional scale. However, a major setback would be the comparatively coarse spatial resolution of the NASA-POWER data, which may not accurately capture land-atmosphere processes.

As mean temperature is expected to rise over the Savannah zone (Klutse et al., 2020), this study can provide a framework for water management policies over the region. The expected temperature rise, considering the mono-modal rainfall regime over the Savannah with an average annual total rainfall of 1000 mm (Hill et al., 2016; Asante, Amuakwa-Mensah, 2014), should suggest increasing evapotranspiration and hence a future lower aridity index.

4. Conclusion

This work highlights the successful application of bias correction to NASA-POWER satellite-derived reanalysis datasets, significantly improving their utility for assessing water resource availability in Ghana based on Aridity Index. The bias correction method adopted notably refined the Aridity Index estimates for wetland and dryland climate representation, thus enhancing the R^2 from 0.69 to 0.87, which underscores a strong alignment with in-situ station data. The corrections reduced the mean bias for temperature and rainfall estimations, ensuring that the dataset more accurately reflects the varying climatic conditions across Ghana's distinct zones - from the humid southern regions to the drier northern Savannahs. With these improvements, the NASA-POWER data now offer a more reliable basis for water resource management strategies, capable of accommodating the spatial and temporal climatic diversity of the

Table 3
Summary of monthly mean values of long-term climate data derived from the Ghana Meteorological Agency (GMet) and the NASA-POWER reanalysis archives.

Variable	Unit	GMet	NASA-POWER	Absolute Bias Correction	
				Before	After
T_{min}	℃	22.8	19.55	3.24	0.12
T_{max}	℃	32.01	35.48	3.39	0.14
R	mm	3.08	3.45	0.37	0.001

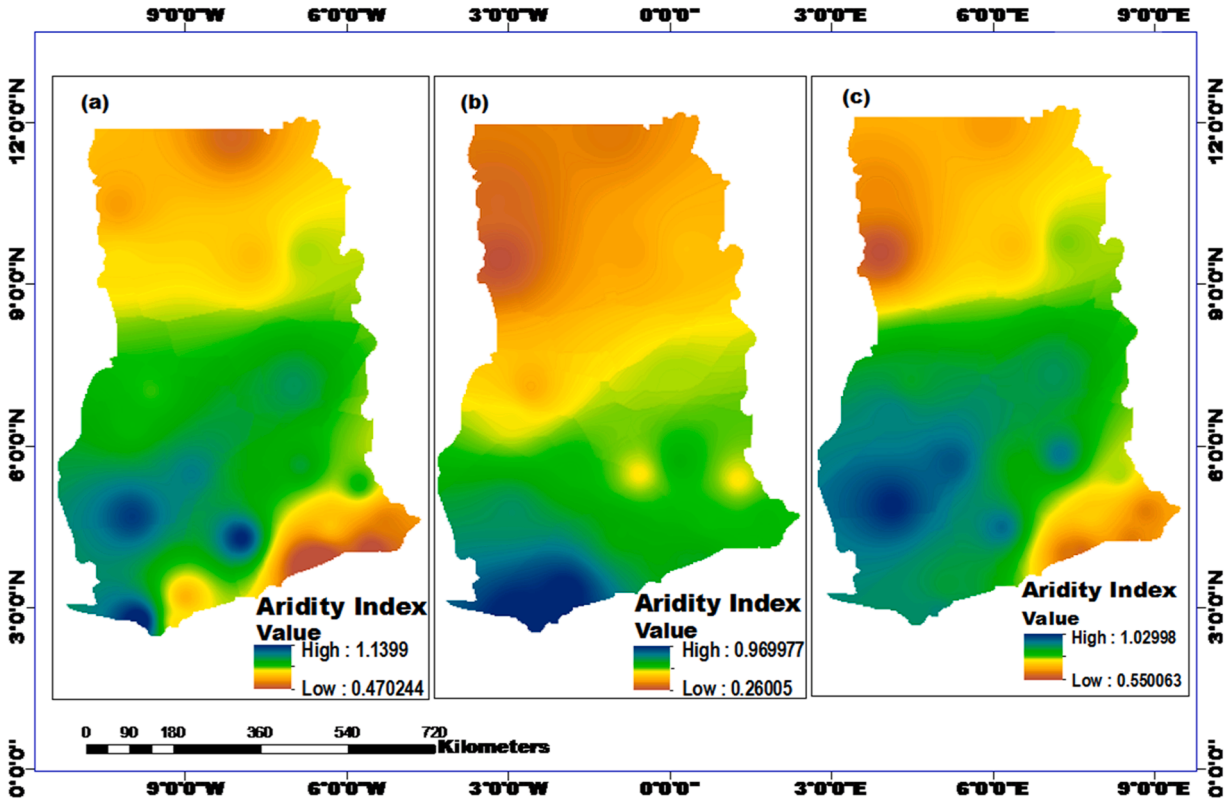

Fig. 5. Spatiial maps of airidity index distribution derived from (a) station measurment data, (b) NASA-POWER data, and (c) corrected NASA-POWER data.

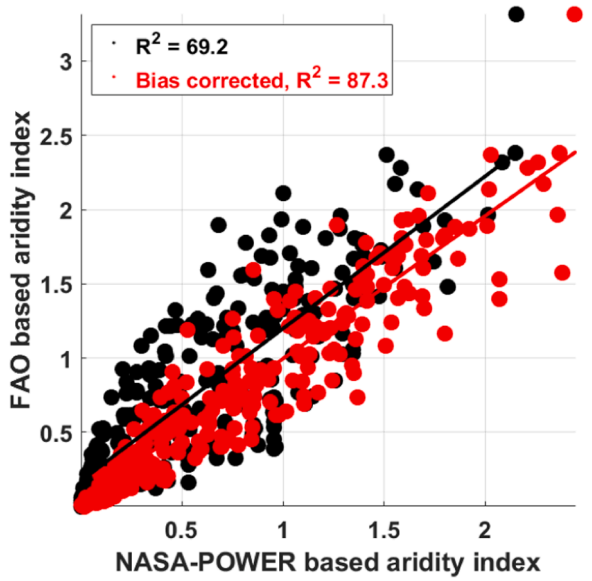

Fig. 6. Comparing the performance of NASA-POWER based aridity estimation for each synoptic station before and after bias correction.

region. This methodology provides a robust framework for other regions to enhance the precision of satellite data, facilitating more informed decision-making in the face of climatic uncertainties.

CRediT authorship contribution statement

Asilevi Prince Junior: Writing – review & editing, Writing – original draft, Visualization, Validation, Software, Resources, Methodology, Investigation, Formal analysis, Data curation, Conceptualization. **Aryee Jeffrey Nii Armah:** Software, Visualization, Writing – review & editing. **Boakye Patrick:** Project administration, Methodology, Funding acquisition. **Owusu Stephen:** Writing – review & editing. **Amekudzi Leonard Kofitse:** Supervision, Writing – review & editing. **Peprah David Kofi:** Data curation, Visualization. **Dogbey Felicia:** Visualization, Software, Resources, Methodology, Formal analysis. **Bentum John:** Validation, Supervision, Resources. **Anornu Geophrey:** Validation, Supervision, Resources. **Quansah Emmanuel:** Writing – review & editing, Validation, Supervision, Resources, Methodology. **Yamba Edmund:** Writing – review & editing. **Klutse Nana:** Validation, Supervision. **Oduro-Kwarteng Sampson:** Supervision, Resources. **Adjei Kwaku:** Validation, Supervision, Resources.

Declaration of Competing Interest

The authors declare no competing interests.

Data Availability

Data will be made available on request. The datasets generated during and/or analyzed during the current study are available from the corresponding author on reasonable request.

Acknowledgements

We are thankful for the NASA - POWER temperature and rainfall reanalysis products obtained from the NASA Langley Research Center POWER Project funded through the NASA Earth Science Directorate Applied Science Program. Also, we are thankful for the temperature and rainfall measurement datasets from the Ghana Meteorological Agency (GMet).

We appreciate the support by the Regional Water and Environmental Sanitation Centre Kumasi (RWESCK), of the Kwame Nkrumah University of Science and Technology (KNUST).

Author contributions

Conceptualization, P. J. A., F. D., and P. B* ; methodology, P. J. A., and F. D.; data curation, P. J. A., S. Y. O.; writing-original draft, P. J. A.; writing-review & editing, S. Y. O., S. O. K., N. A. B. K., K. A. A., G. K. A., J. K. B., J.N.A.A., D.K.P, E. I. Y., E. Q., and L.K.A; funding acquisition, P. B* .

References

Afzaal, H., Farooque, A.A., Abbas, F., Acharya, B., Esau, T., 2020. Computation of evapotranspiration with artificial intelligence for precision water resource management. Appl. Sci. 10, 1621. https://doi.org/10.3390/app10051621.

Ahanhanzo, C., Johnson, E.A.K., Eboreime, E.A., Issiaka, S., Traoré, B.I., Adohinzin, C.C., Okolo, S., 2021. COVID-19 in West Africa: regional resource mobilisation and allocation in the first year of the pandemic. BMJ Glob. Health 6 (5), e004762. https://doi.org/10.1136/bmjgh-2020-004762.

Allen, R.G., Pereira, L.S., Raes, D., Smith, M., 1998. Guidelines for computing crop water requirements-FAO Irrigation and drainage paper 56, FAO-Food and Agriculture Organisation of the United Nations, Rome (http://www. fao. org/docrep) ARPAV (2000), La caratterizzazione climatica della Regione Veneto, Quaderni per. Geophysics 156 (178).

Amekudzi, L.K., Yamba, E.I., Preko, K., Asare, E.O., Aryee, J., Baidu, M., Codjoe, S.N., 2015. Variabilities in rainfall onset, cessation, and length of rainy season for the various agro-ecological zones of Ghana. Climate 3, 416–434. https://doi.org/10.3390/cli3020416.

Anderson, M.C., Allen, R.G., Morse, A., Kustas, W.P., 2012. Use of Landsat thermal imagery in monitoring evapotranspiration and managing water resources. Remote Sens. Environ. 122, 50–65. https://doi.org/10.1016/j.rse.2011.08.025.

Asante, F.A., Amuakwa-Mensah, F., 2014. Climate change and variability in Ghana: Stocktaking. Climate 3, 78–101. https://doi.org/10.3390/cli3010078.

Asilevi Junior, P., Opoku, N.K., Martey, F., Setsoafia, E., Ahafianyo, F., Quansah, E., Padi, M., 2022. Development of high-resolution cloud cover climatology databank using merged manual and satellite datasets over Ghana, West Africa. Atmosphere-Ocean 1–14. https://doi.org/10.1080/07055900.2022.2072266.

Bai, J., Chen, X., Dobermann, A., Yang, H., Cassman, K.G., Zhang, F., 2010. Evaluation of NASA satellite-and model-derived weather data for simulation of maize yield potential in China. Agron. J. 102, 9–16. https://doi.org/10.2134/agronj2009.0085.

Bannayan, M., Sanjani, S., Alizadeh, A., Lotfabadi, S.S., Mohamadian, A., 2010. Association between climate indices, aridity index, and rainfed crop yield in northeast of Iran. Field Crops Res. 118, 105–114. https://doi.org/10.1016/j.fcr.2010.04.011.

Boltz, F., Poff, N.L., Folke, C., Kete, N., Brown, C.M., Freeman, S.S.G., Rockström, J., 2019. Water is a master variable: Solving for resilience in the modern era. Water Secur. 8, 100048 https://doi.org/10.1016/j.wasec.2019.100048.

Brandt, M., Tucker, C.J., Kariryaa, A., Rasmussen, K., Abel, C., Small, J., Fensholt, R., 2020. An unexpectedly large count of trees in the West African Sahara and Sahel. Nature 587 (7832), 78–82. https://doi.org/10.1038/s41586-020-2824-5.

Córdova, M., Carrillo-Rojas, G., Crespo, P., Wilcox, B., Célleri, R., 2015. Evaluation of the penman-monteith (FAO 56 PM) method for calculating reference evapotranspiration using limited data. Mt. Res. Dev. 35, 230–239. https://doi.org/10.1659/MRD-JOURNAL-D-15-0024.S1.

Danso, D.K., Anquetin, S., Diedhiou, A., Lavaysse, C., Kobea, A., Touré, N.D.E., 2019. Spatio-temporal variability of cloud cover types in West Africa with satellite-based and reanalysis data. Q. J. R. Meteorol. Soc. 145, 3715–3731. https://doi.org/10.1002/qj.3651.

Dile, Y.T., Ayana, E.K., Worqlul, A.W., Xie, H., Srinivasan, R., Lefore, N., Clarke, N., 2020. Evaluating satellite-based evapotranspiration estimates for hydrological applications in data-scarce regions: a case in Ethiopia. Sci. Total Environ. 743, 140702 https://doi.org/10.1016/j.scitotenv.2020.140702.

Dinku, T., Faniriantsoa, R., Islam, S., Nsengiyumva, G., Grossi, A., 2022. The climate data tool: enhancing climate services across Africa. Front. Clim. 185 https://doi.org/10.3389/fclim.2021.787519.
Droogers, P., Allen, R.G., 2002. Estimating reference evapotranspiration under inaccurate data conditions. Irrig. Drain. Syst. 16, 33–45. https://doi.org/10.1023/A:1015508322413.
Du, J., Fu, Q., Fang, S., Wu, J., He, P., Quan, Z., 2019. Effects of rapid urbanization on vegetation cover in the metropolises of China over the last four decades. Ecol. Indic. 107, 105458 https://doi.org/10.1016/j.ecolind.2019.105458.
Exner-Kittridge, M.G., Rains, M.C., 2010. Case study on the accuracy and cost/effectiveness in simulating reference evapotranspiration in West-Central Florida. J. Hydrol. Eng. 15, 696–703. https://doi.org/10.1061/(ASCE)HE.1943-5584.0000239.
Fooladmand, H.R., Haghighat, M., 2007. Spatial and temporal calibration of Hargreaves equation for calculating monthly ETo based on Penman-Monteith method. Irrig. Drain.: J. Int. Comm. Irrig. Drain. 56, 439–449. https://doi.org/10.1002/ird.305.
Garcia, M., Raes, D., Allen, R., Herbas, C., 2004. Dynamics of reference evapotranspiration in the Bolivian highlands (Altiplano). Agric. For. Meteorol. 125, 67–82. https://doi.org/10.1016/j.agrformet.2004.03.005.
Gebremedhin, M.A., Kahsay, G.H., Fanta, H.G., 2018. Assessment of spatial distribution of aridity indices in Raya valley, northern Ethiopia. Appl. Water Sci. 8 (8), 1. https://doi.org/10.1007/s13201-018-0868-6.
Gocic, M., Trajkovic, S., 2010. Software for estimating reference evapotranspiration using limited weather data. Comput. Electron. Agric. 71, 158–162. https://doi.org/10.1016/j.compag.2010.01.003.
Greene, C.A., Thirumalai, K., Kearney, K.A., Delgado, J.M., Schwanghart, W., Wolfenbarger, N.S., Blankenship, D.D., 2019. The climate data toolbox for MATLAB. Geochem., Geophys., Geosystems 20, 3774–3781. https://doi.org/10.1029/2019GC008392.
Greve, P., Kahil, T., Mochizuki, J., Schinko, T., Satoh, Y., Burek, P., Wada, Y., 2018. Global assessment of water challenges under uncertainty in water scarcity projections. Nat. Sustain. 1, 486–494. https://doi.org/10.1038/s41893-018-0134-9.
Gudmundsson, L., Greve, P., Seneviratne, S.I., 2016. The sensitivity of water availability to changes in the aridity index and other factors—A probabilistic analysis in the Budyko space. Geophysical Research Letters, 43 (13), 6985–6994. https://doi.org/10.1002/2016GL069763.
Hargreaves, G.H., Samani, Z.A., 1985. Reference crop evapotranspiration from temperature. Appl. Eng. Agric. 1, 96–99. https://doi.org/10.13031/2013.26773.
Hill, P.G., Allan, R.P., Chiu, J.C., Stein, T.H., 2016. A multisatellite climatology of clouds, radiation, and precipitation in southern West Africa and comparison to climate models. J. Geophys. Res.: Atmospheres 121, 10–857. https://doi.org/10.1002/2016JD025246.
Hill, P.G., Allan, R.P., Chiu, J.C., Bodas-Salcedo, A., Knippertz, P., 2018. Quantifying the contribution of different cloud types to the radiation budget in southern West Africa. J. Clim. 31, 5273–5291. https://doi.org/10.1175/JCLI-D-17-0586.1.
Hou, L.G., Zou, S.B., Xiao, H.L., Yang, Y.G., 2013. Sensitivity of the reference evapotranspiration to key climatic variables during the growing season in the Ejina oasis northwest China. In: SpringerPlus, Vol. 2. SpringerOpen,, pp. 1–6. https://doi.org/10.1186/2193-1801-2-S1-S4.
Igbadun, H., Mahoo, H., Tarimo, A.K.P.R., Salim, B. Performance of two temperature-based reference evapotranspiration models in the Mkoji sub-catchment in Tanzania (2006). https://hdl.handle.net/1813/10226.
Jung, M., Reichstein, M., Ciais, P., Seneviratne, S.I., Sheffield, J., Goulden, M.L., Zhang, K., 2010. Recent decline in the global land evapotranspiration trend due to limited moisture supply. Nature 467, 951–954. https://doi.org/10.1038/nature09396.
Khosravi, K., Daggupati, P., Alami, M.T., Awadh, S.M., Ghareb, M.I., Panahi, M., Yaseen, Z.M., 2019. Meteorological data mining and hybrid data-intelligence models for reference evaporation simulation: a case study in Iraq. Comput. Electron. Agric. 167, 105041 https://doi.org/10.1016/j.compag.2019.105041.
Klutse, N.A.B., Owusu, K., Boafo, Y.A., 2020. Projected temperature increases over northern Ghana. SN Appl. Sci. 2, 1–14. https://doi.org/10.1007/s42452-020-3095-3.
Li, Z., Zheng, F.L., Liu, W.Z., 2012. Spatiotemporal characteristics of reference evapotranspiration during 1961–2009 and its projected changes during 2011–2099 on the Loess Plateau of China. Agric. For. Meteorol. 154, 147–155. https://doi.org/10.1016/j.agrformet.2011.10.019.
Liu, X., Zhang, D., Luo, Y., Liu, C., 2013. Spatial and temporal changes in aridity index in northwest China: 1960 to 2010. Theor. Appl. Climatol. 112, 307–316. https://doi.org/10.1007/s00704-012-0734-7.
Liu, Y., Xue, Y., 2020. Expansion of the Sahara Desert and shrinking of frozen land of the Arctic. Sci. Rep. 10 (1), 9. https://doi.org/10.1038/s41598-020-61085-0.
López-Urrea, R., de Santa Olalla, F.M., Fabeiro, C., Moratalla, A., 2006. Testing evapotranspiration equations using lysimeter observations in a semiarid climate. Agric. Water Manag. 85, 15–26. https://doi.org/10.1016/j.agwat.2006.03.014.
Mahmoud, M.A., Henderson, G.R., Epprecht, E.K., Woodall, W.H., 2010. Estimating the standard deviation in quality-control applications. J. Qual. Technol. 42 (4), 348–357. https://doi.org/10.1080/00224065.2010.11917832.
Martinez, C.J., Thepadia, M., 2010. Estimating reference evapotranspiration with minimum data in Florida. J. Irrig. Drain. Eng. 136, 494–501. https://doi.org/10.1061/(ASCE)IR.1943-4774.0000214.
Masih, I., Maskey, S., Mussá, F.E.F., Trambauer, P., 2014. A review of droughts on the African continent: a geospatial and long-term perspective. Hydrol. Earth Syst. Sci. 18, 3635–3649. https://doi.org/10.5194/hess-18-3635-2014.
McDonald, R.I., Douglas, I., Revenga, C., Hale, R., Grimm, N., Grönwall, J., Fekete, B., 2011. Global urban growth and the geography of water availability, quality, and delivery. Ambio 40, 437–446. https://doi.org/10.1007/s13280-011-0152-6.
Michelangeli, P.A., Vrac, M., Loukos, H., 2009. Probabilistic downscaling approaches: application to wind cumulative distribution functions. Geophys. Res. Lett. 36 https://doi.org/10.1029/2009GL038401.
Moletto-Lobos, I., Mattar, C., Barichivich, J., 2020. Performance of satellite-based evapotranspiration models in temperate pastures of southern Chile. Water 12, 3587. https://doi.org/10.3390/w12123587.
Molod, A., Takacs, L., Suarez, M., Bacmeister, J., 2015. Development of the GEOS-5 atmospheric general circulation model: Evolution from MERRA to MERRA2. Geosci. Model Dev. 8, 1339–1356. https://doi.org/10.5194/gmd-8-1339-2015.
Monteiro, L.A., Sentelhas, P.C., Pedra, G.U., 2018. Assessment of NASA/POWER satellite-based weather system for Brazilian conditions and its impact on sugarcane yield simulation. Int. J. Climatol. 38, 1571–1581. https://doi.org/10.1002/joc.5282.
Moral, F.J., Rebollo, F.J., Paniagua, L.L., García-Martín, A., Honorio, F., 2016. Spatial distribution and comparison of aridity indices in Extremadura, southwestern Spain. Theor. Appl. Climatol. 126, 801–814. https://doi.org/10.1007/s00704-015-1615-7.
Mu, L., Fang, L., Dou, W., Wang, C., Qu, X., Yu, Y., 2021. Urbanization-induced spatio-temporal variation of water resources utilization in northwestern China: a spatial panel model-based approach. Ecol. Indic. 125, 107457 https://doi.org/10.1016/j.ecolind.2021.107457.
Mueller, B., Seneviratne, S.I., Jimenez, C., Corti, T., Hirschi, M., Balsamo, G., Zhang, Y., 2011. Evaluation of global observations-based evapotranspiration datasets and IPCC AR4 simulations. Geophys. Res. Lett. 38 https://doi.org/10.1029/2010GL046230.
Mueller, B., Hirschi, M., Jimenez, C., Ciais, P., Dirmeyer, P.A., Dolman, A.J., Seneviratne, S.I., 2013. Benchmark products for land evapotranspiration: LandFlux-EVAL multi-data set synthesis. Hydrol. Earth Syst. Sci. 17, 3707–3720. https://doi.org/10.5194/hess-17-3707-2013.
Nagelkerke, N.J., 1991. A note on a general definition of the coefficient of determination. biometrika 78 (3), 691–692. https://doi.org/10.1093/biomet/78.3.691.
Nastos, P.T., Politi, N., Kapsomenakis, J., 2013. Spatial and temporal variability of the Aridity Index in Greece. Atmos. Res. 119, 140–152. https://doi.org/10.1016/j.atmosres.2011.06.017.
Ndehedehe, C.E., Ferreira, V.G., Agutu, N.O., 2019. Hydrological controls on surface vegetation dynamics over West and Central Africa. Ecol. Indic. 103, 494–508. https://doi.org/10.1016/j.ecolind.2019.04.032.
Nkrumah, F., Klutse, N.A.B., Adukpo, D.C., Owusu, K., Quagraine, K.A. Rainfall variability over Ghana: model versus rain gauge observation (2014). ⟨https://doi.org/10.4236/ijg.2014.57060⟩.
Ojeda, J.J., Volenec, J.J., Brouder, S.M., Caviglia, O.P., Agnusdei, M.G., 2017. Evaluation of Agricultural Production Systems Simulator as yield predictor of Panicum virgatum and Miscanthus x giganteus in several US environments. Gcb Bioenergy 9, 796–816. https://doi.org/10.1111/gcbb.12384.
Oki, T., Kanae, S., 2006. Global hydrological cycles and world water resources. science 313, 1068–1072. https://doi.org/10.1126/science.1128845.

Pereira, L.S., Oweis, T., Zairi, A., 2002. Irrigation management under water scarcity. Agric. Water Manag. 57, 175–206. https://doi.org/10.1016/S0378-3774(02)00075-6.

Rahimikhoob, A., Behbahani, M.R., Fakheri, J., 2012. An evaluation of four reference evapotranspiration models in a subtropical climate. Water Resour. Manag. 26, 2867–2881. https://doi.org/10.1007/s11269-012-0054-9.

Rain, D., Engstrom, R., Ludlow, C., Antos, S., 2011. Accra Ghana: a city vulnerable to flooding and drought-induced migration. Case Study Prep. Cities Clim. Chang.: Glob. Rep. Hum. Settl. 2011, 1–21.

Rienecker, M.M., Suarez, M.J., Gelaro, R., Todling, R., Bacmeister, J., Liu, E., Woollen, J., 2011. MERRA: NASA's modern-era retrospective analysis for research and applications. J. Clim. 24, 3624–3648. https://doi.org/10.1175/JCLI-D-11-00015.1.

Savary, S., Nelson, A., Willocquet, L., Pangga, I., Aunario, J., 2012. Modeling and mapping potential epidemics of rice diseases globally. Crop Prot. 34, 6–17. https://doi.org/10.1016/j.cropro.2011.11.009.

Setianto, A., Triandini, T., 2013. Comparison of kriging and inverse distance weighted (IDW) interpolation methods in lineament extraction and analysis. J. Appl. Geol. 5 (1) https://doi.org/10.22146/jag.7204.

Shepard, D., 1968. A two-dimensional interpolation function for irregularly-spaced data. Proc. 1968 23rd ACM Natl. Conf. 517–524. https://doi.org/10.1145/800186.810616.

Singh, A., Gaurav, K., Meena, G.K., Kumar, S., 2020. Estimation of soil moisture applying modified dubois model to Sentinel-1; a regional study from central India. Remote Sens. 12, 2266. https://doi.org/10.3390/rs12142266.

Soro, T., Kouakou, B., Kouassi, E., Soro, G., Kouassi, A., Kouadio, K., Soro, N., 2013. Hydroclimatologie et dynamique de l'occupation du sol du bassin versant du Haut Bandama à Tortiya (Nord de la Côte d'Ivoire). Vertigo.: la Rev. électronique En. Sci. De. l'environnement 13. https://doi.org/10.4000/vertigo.14468.

Stackhouse Jr, P., Eckman, R., Zhang, T., Mikovitz, J., Whitlock, C., Chandler, W., Lilienthal, P., 2006. Supporting energy-related societal applications using NASAs satellite and modeling data (July). 2006 IEEE International Symposium on Geoscience and Remote Sensing. IEEE,, pp. 425–428. https://doi.org/10.1109/IGARSS.2006.113 (July).

Stöckle, C.O., Kjelgaard, J., Bellocchi, G., 2004. Evaluation of estimated weather data for calculating Penman-Monteith reference crop evapotranspiration. Irrig. Sci. 23, 39–46. https://doi.org/10.1007/s00271-004-0091-0.

Suarez, M.J., daSilva, A., Dee, D., Bloom, S., Bosilovich, M., Pawson, S.,. & Stajner, I. *Documentation and validation of the Goddard Earth Observing System (GEOS) data assimilation system, version 4* (No. Rept-2005–01264-0/VOL26/VER4) (2005).

Susanto, F., de Souza Jr, P., He, J., 2016. Spatiotemporal interpolation for environmental modelling. Sensors 16 (8), 1245. https://doi.org/10.3390/s16081245.

Svoboda, M.D., Fuchs, B.A., 2016. Handbook of drought indicators and indices. World Meteorological Organization,, Geneva, Switzerland, pp. 1–44. https://doi.org/10.1201/9781315265551-12.

Tabari, H., 2010. Evaluation of reference crop evapotranspiration equations in various climates. Water Resour. Manag. 24, 2311–2337. https://doi.org/10.1007/s11269-009-9553-8.

Tabari, H., Talaee, P.H., Nadoushani, S.M., Willems, P., Marchetto, A., 2014. A survey of temperature and precipitation-based aridity indices in Iran. Quat. Int. 345, 158–166. https://doi.org/10.1016/j.quaint.2014.03.061.

Trajkovic, S., Kolakovic, S., 2009. Evaluation of reference evapotranspiration equations under humid conditions. Water Resour. Manag. 23, 3057–3067. https://doi.org/10.1007/s11269-009-9423-4.

White, J.W., Hoogenboom, G., Stackhouse Jr, P.W., Hoell, J.M., 2008. Evaluation of NASA satellite-and assimilation model-derived long-term daily temperature data over the continental US. Agric. For. Meteorol. 148, 1574–1584. https://doi.org/10.1016/j.agrformet.2008.05.017.

Wohl, E., Barros, A., Brunsell, N., Chappell, N.A., Coe, M., Giambelluca, T., Ogden, F., 2012. The hydrology of the humid tropics. Nat. Clim. Change 2, 655–662. https://doi.org/10.1038/nclimate1556.

Xing, Z., Chow, L., Meng, F.R., Rees, H.W., Stevens, L., Monteith, J., 2008. Validating evapotranspiraiton equations using bowen ratio in New Brunswick, Maritime, Canada. Sensors 8, 412–428. https://doi.org/10.3390/s8010412.

Xu, J., Peng, S., Ding, J., Wei, Q., Yu, Y., 2013. Evaluation and calibration of simple methods for daily reference evapotranspiration estimation in humid East China. Arch. Agron. Soil Sci. 59, 845–858. https://doi.org/10.1080/03650340.2012.683425.

Zhan, S., Song, C., Wang, J., Sheng, Y., Quan, J., 2019. A global assessment of terrestrial evapotranspiration increases due to surface water area change. Earth'S. Future 7, 266–282. https://doi.org/10.1029/2018EF001066.

Zhang, D., Sial, M.S., Ahmad, N., Filipe, A.J., Thu, P.A., Zia-Ud-Din, M., Caleiro, A.B., 2020. Water scarcity and sustainability in an emerging economy: a management perspective for future. Sustainability 13, 144. https://doi.org/10.3390/su13010144.

Zhang, T., Chandler, W.S., Hoell, J.M., Westberg, D., Whitlock, C.H., Stackhouse, P.W., 2008. A global perspective on renewable energy resources: NASA's prediction of worldwide energy resources (power) project. Proceedings of ISES World Congress 2007 (Vol. I–Vol. V). Springer,, Berlin, Heidelberg, pp. 2636–2640. https://doi.org/10.1007/978-3-540-75997-3_532.